BIOCHEMISTRY
including biophysical chemistry & molecular biology

Article

pubs.acs.org/biochemistry

Dual Role of the Active Site Residues of *Thermus thermophilus* 3-Isopropylmalate Dehydrogenase: Chemical Catalysis and Domain Closure

Éva Gráczer,[†] Tamás Szimler,[†] Anita Garamszegi,[†] Petr V. Konarev,[‡,#] Anikó Lábas,[§] Julianna Oláh,[*,§] Anna Palló,[∥] Dmitri I. Svergun,[‡] Angelo Merli,[⊥] Péter Závodszky,[†] Manfred S. Weiss,[@] and Mária Vas[*,†]

[†]Institute of Enzymology, Research Centre for Natural Sciences, Hungarian Academy of Sciences, Magyar tudósok krt. 2., H-1117 Budapest, Hungary

[‡]European Molecular Biology Laboratory, Hamburg Outstation, Notkestrasse 85, 22603 Hamburg, Germany

[§]Department of Inorganic and Analytical Chemistry, Budapest University of Technology and Economics, Gellért tér 4., H-1111 Budapest, Hungary

[∥]Institute of Organic Chemistry, Research Centre for Natural Sciences, Hungarian Academy of Sciences, Magyar tudósok krt. 2., H-1117 Budapest, Hungary

[⊥]Dipartimento di Bioscienze, Universitá degli Studi di Parma, Viale G.P. Usberti 23/A, I-43100 Parma, Italy

[@]Macromolecular Crystallography (HZB-MX), Helmholtz-Zentrum Berlin für Materialien und Energie, Albert-Einstein-Strasse 15, D-12489 Berlin, Germany

Supporting Information

ABSTRACT: The key active site residues K185, Y139, D217, D241, D245, and N102 of *Thermus thermophilus* 3-isopropylmalate dehydrogenase (*Tt*-IPMDH) have been replaced, one by one, with Ala. A drastic decrease in the k_{cat} value (0.06% compared to that of the wild-type enzyme) has been observed for the K185A and D241A mutants. Similarly, the catalytic interactions (K_m values) of these two mutants with the substrate IPM are weakened by more than 1 order of magnitude. The other mutants retained some (1−13%) of the catalytic activity of the wild-type enzyme and do not exhibit appreciable changes in the substrate K_m values. The pH dependence of the wild-type enzyme activity (pK = 7.4) is shifted toward higher values for mutants K185A and D241A (pK values of 8.4 and 8.5, respectively). For the other mutants, smaller changes have been observed. Consequently, K185 and D241 may constitute a proton relay system that can assist in the abstraction of a proton from the OH group of IPM during catalysis. Molecular dynamics simulations provide strong support for the neutral character of K185 in the resting state of the enzyme, which implies that K185 abstracts the proton from the substrate and D241 assists the process via electrostatic interactions with K185. Quantum mechanics/molecular mechanics calculations revealed a significant increase in the activation energy of the hydride transfer of the redox step for both D217A and D241A mutants. Crystal structure analysis of the molecular contacts of the investigated residues in the enzyme−substrate complex revealed their additional importance (in particular that of K185, D217, and D241) in stabilizing the domain-closed active conformation. In accordance with this, small-angle X-ray scattering measurements indicated the complete absence of domain closure in the cases of D217A and D241A mutants, while only partial domain closure could be detected for the other mutants. This suggests that the same residues that are important for catalysis are also essential for inducing domain closure.

Activity (k_{cat}, min^{-1}) of IPMDH	
Wild-type	238 +/- 30
K185A	0.15 +/- 0.05
D241A	0.15 +/- 0.05
D217A	2.7 +/- 0.5

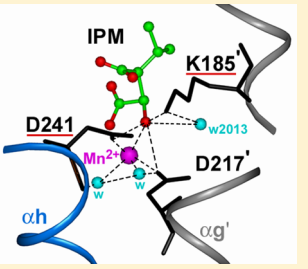

3-Isopropylmalate dehydrogenase (IPMDH) is a member of the β-hydroxyacid oxidative decarboxylase family, to which also isocitrate dehydrogenase, homoisocitrate dehydrogenase, tartarate dehydrogenase, and malic enzyme belong (cf. ref 1 for a review). Evidence from structural,[2−4] bioinformatics,[1] and biochemical studies (mutation analysis, pH profiles, etc.)[4−8] suggests that the catalytic apparatus of these related enzymes are similar (including the critical role of a Lys-Tyr pair), although there may be some uncertainties concerning the role of each amino acid side chain in the active site. In particular, contradictory conclusions were drawn about the contribution of the active site aspartates in the catalysis by isocitrate dehydrogenase. As for IPMDH, functional studies based on mutational analysis are rather scarce,[10−12] and the role of the active site Lys and Asp sid -chains has not yet been tested.

Received: July 24, 2015
Revised: December 10, 2015

DOI: 10.1021/acs.biochem.5b00839
Biochemistry XXXX, XXX, XXX−XXX

IPMDH catalyzes the oxidation and decarboxylation of (2*R*,3*S*)-3-isopropylmalate (IPM) to 2-oxo-4-methyl-pentanoate (2-oxo-isocaproate) in the presence of NAD^+ and a divalent cation (Mn^{2+} or Mg^{2+}) in the leucine biosynthetic pathway of bacteria, fungi, and plants. The role of K185 of *Thermus thermophilus* (*Tt*) IPMDH, a conserved active site residue, as a catalytic base in aiding deprotonation of the OH group of the substrate IPM has been recently proposed, on the basis of evidence from the completely closed crystal structure of the nonfunctioning *Tt*-IPMDH–Mn^{2+}–IPM–NADH quaternary complex in combination with quantum mechanics/molecular mechanics (QM/MM) calculations.[13] This notion is in accordance with the previous suggestion of the catalytic role of the invariant K230 of *Escherichia coli* isocitrate dehydrogenase.[4] In the work presented here, besides this Lys (K185 in *Tt*-IPMDH), we directly investigate the roles of other conserved active site residues (Y139, D217, D241, D245, and N102) of *Tt*-IPMDH by site-directed mutagenesis. All these residues, except N102, are in direct contact with the substrate. The side chain of N102, however, was suggested to contribute to the activity through regulating the communication of the two domains.[14]

Indeed, in addition to the possible participation of these active site side chains in the chemical catalysis, a further exciting aspect is their simultaneous involvement in the allosteric regulation of domain closure that leads to the optimal alignment of the reacting substrates. In general, there are many examples of proteins/enzymes where domain movements are evidenced as an integral part of their function (e.g., refs 15–25). In fact, mechanisms of domain movement are considered to be among the most general problems of both enzymology and protein chemistry: operation of hinge bending or shearing motion of domains and the route of allosteric propagation of the effects of substrates toward the hinges or shearing surfaces by participating important conserved side chains deserve wide interest. Hinges between the two domains have been identified in cases of oxidative decarboxylases, such as the malic enzyme,[26] isocitrate dehydrogenase,[4] tartrate dehydrogenase,[3] and IPMDH.[14] However, an open question discussed in several reviews is how the allosteric effects of the bound substrates are propagated within a protein molecule toward the molecular hinges. In other words, the structural principles (definitive, longer/shorter allosteric pathways from the substrate binding sites) that govern movement of hinges in most cases have not been clarified.

In this work, besides identifying the important catalytic residues of *Tt*-IPMDH, we aimed to elaborate possible conformational pathways through which their molecular contacts may lead to domain closure. These suggested mechanisms are also tested and confirmed by FRET and SAXS measurements conducted with the respective mutants.

MATERIALS AND METHODS

Enzymes and Chemicals. The conserved active site residues (K185, Y139, D217, D241, D245, and N102) of *Tt*-IPMDH were mutated to Ala using the QuickChange site-directed mutagenesis kit. The modified enzymes were expressed and purified using the previously published method applied for the wild-type enzyme.[30] (2*R*,3*S*)-3-Isopropylmalic acid (IPM) was purchased from Wako Biochemicals (Japan), and NAD^+ and NADH were from Sigma. All other chemicals were commercially available high-purity grade products.

SDS–PAGE and Native Gel Electrophoresis. SDS gel electrophoresis was conducted using the method of Laemmli.[31] Native gel electrophoresis was performed using the method of Ornstein.[32] The resolving and stacking gels were 12.5 and 5%, respectively. IPMDH (3 μg) was loaded into the gel, and the electrophoresis was conducted at 180 V in a buffer of pH 8.3 for 1 h. The gels were stained with Coomassie Brilliant Blue G-250.

Far- and Near-UV CD Spectra. CD measurements were performed with a Jasco J-720 spectropolarimeter equipped with a Neslab RTE 111 computer-controlled thermostat. Far-UV CD spectra were recorded in the range of 190–260 nm; the cuvette with a 1 mm path length was used at a protein concentration of 0.6 mg/mL (15 μM monomer). For recording near-UV CD spectra in the range of 260–350 nm, the cuvette with a 1 cm path length was used at a protein concentration of 1.5 mg/mL (40 μM monomer).

Enzyme Kinetic Studies. Activity of IPMDH (wild type, 6–12 μg/mL, i.e., 0.16–0.32 μM monomer; or various mutants, ranging from 0.1 to 10 mg/mL, i.e., 2.6–260 μM) was assayed in the presence of 0.5 mM IPM, 0.5 mM $MnCl_2$, and 4 mM NAD in 25 mM MOPS-KOH buffer (pH 7.6). When required (e.g., in the cases of K185A, D241A, and D245A mutants), the activities were assayed in the presence of excess (up to 500 mM) KCl. The formation of NADH was recorded spectrophotometrically at 340 nm and 20 °C using a Jasco (Tokyo, Japan) V-550 spectrophotometer equipped with a Grant Y6 thermostat. The substrate K_m values were determined at varying concentrations of each substrate, while keeping constant and closely saturating concentrations of the other substrates. The kinetic data were fitted using the Michaelis–Menten equation.

Dependence of Enzyme Activity on pH. Enzyme activities were tested at various pHs using the following buffers: 25 mM MES-NaOH (pH range of 6.0–6.6), 25 mM MOPS-NaOH (pH range of 6.0–8.0), 10 mM HEPES-NaOH (pH range of 7.0–8.0), 50 mM Tris-HCl (pH range of 7.5–9.0), and 50 mM diethanolamine-HCl (pH range of 8.7–10.0). The overlapping pH ranges of the particular buffers assured elimination of any influence of the specific buffer components on enzyme activity. To test whether substrates are applied at closely saturating concentrations, the measurements at each pH were repeated at various high concentrations of each substrate. The experimental activity values as a function of pH were determined and fitted according to the Henderson–Hasselbach equation of a simple deprotonation dissociation curve:

$$\nu_{\text{measured}} = \frac{\nu_{\text{extrapolated}}}{1 + 10^{-(\text{pH}-\text{p}K)}} \quad (1)$$

where ν_{measured} is the the activity value measured at a given pH, $\nu_{\text{extrapolated}}$ is the maximal activity value extrapolated to the high pH range, and pK is the characteristic of a catalytic dissociating basic or acidic side chain involved in the catalytic reaction.

FRET Measurements. The Förster resonance energy transfer (FRET) between Trp(s) of IPMDH and the bound NADH was recorded at 20 °C in the presence of Mg^{2+}-IPM as reported by Dean and Dvorak[10] using a SPEX Fluoromax-3 spectrofluorimeter equipped with a Peltier (Edison, NJ) thermostat. The usual mixture contained 24 μg/mL (0.64 μM monomer) IPMDH (wild type or mutant) 12 μM NADH, 3 mM $MgCl_2$, 1 mM IPM, and excess (≤500 mM) KCl. The protein was excited at 295 nm, and the emission was recorded between 300 and 550 nm in a cuvette with a path length of 10

DOI: 10.1021/acs.biochem.5b00839
Biochemistry XXXX, XXX, XXX–XXX

mm. Slits of 2 and 4 nm were applied for excitation and emission, respectively.

SAXS Measurements and Data Processing. Synchrotron radiation solution X-ray scattering data were collected on beamline P12 at the Hamburg EMBL Outstation (on the PETRA III storage ring, at DESY). Solutions of complexes of the wild type and the various mutants of *Tt*-IPMDH with Mn^{2+}-IPM and NADH (nonfunctioning complex) in 25 mM MOPS-NaOH buffer (pH 7.6) (cf. Table 2) were measured at protein concentrations in the range of 5.0−10 mg/mL using a pixel 2M PILATUS detector (DECTRIS) at a sample−detector distance of 3.1 m and a wavelength λ of 1.25 Å, covering the momentum transfer (s) range of 0.01−0.45 $Å^{-1}$ [$s = 4\pi \sin(\theta)/\lambda$, where 2θ is the scattering angle]. The concentrations of Mn^{2+}, IPM, and NADH in the protein samples were 1, 0.5, and 5 mM, respectively. To check for radiation damage, results of 20 exposures of 50 ms each were compared; no radiation damage effects were observed. The data, after normalization to the intensity of the incident beam, were averaged, and the scattering of the buffer was subtracted. All data manipulations were performed using the program package PRIMUS.[33]

Structural parameters, forward scattering $I(0)$, and the radius of gyration R_g were evaluated using the Guinier approximation[34] and the program GNOM.[35] The radii of gyration and the scattering patterns from the crystallographic models of wild-type apo *Tt*-IPMDH [Protein Data Bank (PDB) entry 2Y3Z] and its *Tt*-IPMDH−Mn^{2+}−IPM−NADH substrate complex (PDB entry 4F7I) were computed using the program CRYSOL.[36] The program OLIGOMER[33] was used to calculate the ratio of open- and closed-form species present in *Tt*-IPMDH solutions as described previously.[37]

Molecular Graphical Analysis of the X-ray Structure. The X-ray coordinates of the completely closed structure of the *Tt*-IPMDH−Mn^{2+}−IPM−NADH quaternary complex (PDB entry 4F7I) were used for molecular graphical analysis with the aid of Insight II 95.0 (Biosym/MSI, San Diego, CA). The upper distance limit for hydrogen bonds was taken to be 3.5 Å, while for hydrophobic and ionic interactions, it was considered to be 4.5 Å.

MD Simulations. To assess the most likely protonation state of the side chains of the D217, D241, and K185 residues and of the hydroxyl group of IPM, four different systems were studied and are illustrated in Figure 4A. Five-nanosecond stochastic boundary MD simulations were conducted on each system using the CHARMM software package[38] according to the previously published protocol,[13] which is also described in detail in the Supporting Information.

QM/MM Calculations. To test the contribution of the experimentally mutated side chains in enhancing the catalytic activity of the enzyme, the QM/MM energy profiles obtained earlier for the wild-type enzyme were reinvestigated using point-charge deletion analysis (differential transition state analysis).[39−45] This methodology allowed us to test the electrostatic effect of the mutated side chains on the reaction mechanism, which is considered as the basis of the catalytic effect of enzymes by Warshel and co-workers.[46] The Mn^{2+} ion-bound structures of the wild-type enzyme were taken from our previous study.[13] In that study, we showed that the proton and hydride transfer reactions occur sequentially and determined the reaction barrier of these processes. The effect of the electrostatic environment on the reaction energetics was sampled by investigating the reaction mechanism starting from three structures taken from the trajectory of a 5 ns molecular dynamics simulation. From the three starting structures, three parallel energy profiles (profiles 1, 2, and 3) were determined. In this work, all three parallel profiles were reinvestigated in the case of the WT and mutated enzymes. The representative structures of the reactant (R), intermediate ($I_{hydride}$), transition state (TS1 and TS2), and product ($P_{hydride}$), which is the product of the hydride transfer step and at the same time is the most important intermediate (I) of the overall catalytic cycle, of the Y139A, D217A, D241A, D245A, and N102A point mutants were generated by introducing the corresponding mutation *in silico* by annihilating the charges of the corresponding residues leaving an alanine residue in the systems. This ensured that the observed effects are due to the electrostatic effect of the investigated mutations and do not arise from sampling problems. This procedure yielded three−three structures for each state [R, TS, $I_{hydride}$, TS2, and $I(P_{hydride})$] and for each mutant (altogether $3 \times 5 \times 5 = 75$ structures). Then we conducted QM/MM energy calculations at the B3LYP/6-31G*/MM level of theory using the QoMMMa program[47] that couples the input and output files generated by the Gaussian 09[48] and TINKER[49] program packages. The quantum mechanically described region included the IPM molecule, the nicotinamide ring of NAD^+ with the ribose moiety directly attached to it, K185′ (the prime denotes the side chain from the other subunit), and a water molecule (w2013) located close to both IPM and K185′ (this corresponds to the QM1 region in our previous work[13]). In the work presented here, we decided to use this QM region that is smaller than the one used in our previous work (QM2) because several mutated amino acids belong to the first coordination sphere of Mn^{2+} and as a consequence the manganese ion would lack important ligands, and if it was described quantum mechanically, which would most likely lead to erroneous results. However, this problem does not arise if Mn^{2+} is described by molecular mechanics, more specifically by its charge and Lennard-Jones parameters that usually provide a good description of the nonbonding interaction.

Once the relative energy of each state along the three parallel profiles calculated for each mutated enzyme was determined, we calculated how much the relative energy of each state is modified by the mutations using eq 2:

$$\Delta\Delta E^{\text{mutant}}_{\text{state,profile}} = \Delta E^{\text{mutant}}_{\text{state,profile}} - \Delta E^{\text{WT}}_{\text{state,profile}} \quad (2)$$

over all states (R, TS1, $I_{hydride}$, TS2, and $P_{hydride}$), all profiles (1−3), and all mutants. After this, we calculated the average value ($\overline{\Delta\Delta E^{\text{mutant}}_{\text{state}}}$) and the standard deviation (SD) of these increments over the three profiles and added them to the relative energies calculated for the corresponding WT structures for profile 2 ($\Delta E^{\text{WT}}_{\text{state,2}}$) (see eq 3) to obtain the relative energy of the mutant enzyme ($\Delta E^{\text{mutant}}_{\text{state}}$) in a given state:

$$\Delta E^{\text{mutant}}_{\text{state}} = \Delta E^{\text{WT}}_{\text{state,2}} + \overline{\Delta\Delta E}^{\text{mutant}}_{\text{state,}} \quad (3)$$

From the obtained activation energy differences between the wild-type and point-mutated enzymes, the capability of the studied side chains to stabilize and/or destabilize the transition state via electrostatic interactions can be estimated. If the annihilation of the charges of a given residue leads to higher activation energies, it implies that the given side chain is electrostatically responsible for stabilization of the transition state and is important for catalysis. On the other hand, if no significant increase in the activation energy is observed, it

DOI: 10.1021/acs.biochem.5b00839
Biochemistry XXXX, XXX, XXX−XXX

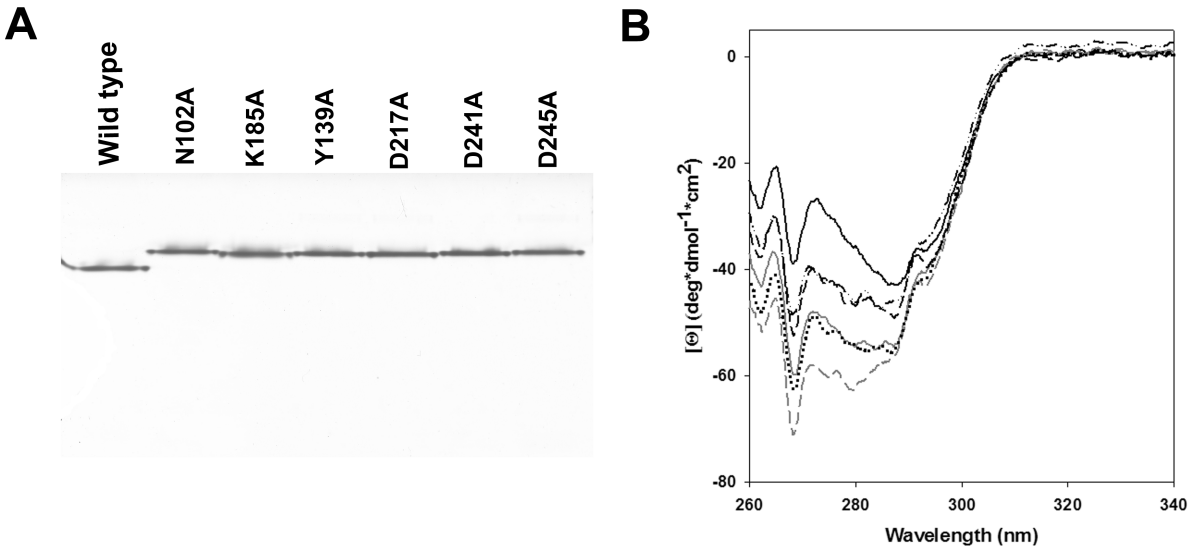

Figure 1. (A) Native gel electrophoresis pattern and (B) near-UV CD spectra of the investigated active site mutants of *Tt*-IPMDH. The experimental details are given in Materials and Methods. In panel B, the near-UV CD spectra of the wild-type enzyme (—) as well as mutants D241A (– – –), D217A (···), D245A (–·–), K185A (gray line), and Y139A (gray dashed line) are illustrated.

Table 1. Kinetic Parameters of the Various Single-Side Chain Mutants of *Tt*-IPMDH[a]

Tt-IPMDH	k_{cat} (min^{-1})	K_m^{IPM} (μM)	$K_m^{NAD^+}$ (μM)	$K_m^{Mn^{2+}}$ (μM)	p*K* of pH dependence	$\Delta\Delta E^{\ddagger}$ (kcal/mol)
wild type[b]	240 ± 30 (100%)	16 ± 3	290 ± 50	10 ± 4	7.4 ± 0.1	0.0
K185A	0.15 ± 0.05 (0.06%)	145 ± 30	64 ± 7	8 ± 2	8.4 ± 0.2	4.3
Y139A	6.5 ± 2.0 (2.7%)	40 ± 9	60 ± 12	28 ± 5	–	2.1
D217A	2.7 ± 0.5 (1.1%)	13 ± 3	305 ± 50	49 ± 7	7.9 ± 0.1	2.6
D241A	0.15 ± 0.05 (0.06%)	255 ± 40	320 ± 50	48 ± 8	8.5 ± 0.2	4.3
D245A	26 ± 8 (10.9%)	20 ± 5	375 ± 60	23 ± 5	7.9 ± 0.1	1.3
N102A	33 ± 8 (13.9%)	14 ± 5	260 ± 80	32 ± 5	nd[d]	1.1
E270A[c]	1.96 ± 0.3 (0.8%)	32 ± 5	660 ± 55	25 ± 6	nd[d]	2.8

[a]Enzyme activities of the wild type and the various mutant forms of IPMDH were measured as described in Materials and Methods. The p*K* values were determined from the pH dependences of the activities by fitting the values to eq 1. The increase in activation energy compared to the wild-type enzyme [$\Delta\Delta E^{\ddagger} = -RT \ln k_{cat}(\text{mutant})/k_{cat}(\text{wild})$] was estimated from the k_{cat} values using the Arrhenius equation and is given in kilocalories per mole. [b]Determined previously.[37,57,62] [c]Determined previously.[57] [d]Not determined.

implies that the given residue does not contribute electrostatically to transition state stabilization of the hydride transfer; however, this does not mean that it cannot be important for catalysis (e.g., through mediation of a protein conformational shift or contributing to the decarboxylation step in the present enzyme), just that our method cannot capture this effect.

■ RESULTS AND DISCUSSION

Physicochemical Properties of the Active Site Mutants of *Tt*-IPMDH. SDS–PAGE of the Ala mutants of selected active site residues of *Tt*-IPMDH illustrated their satisfactory purity. Their native gel electrophoretic pattern further indicates that all the mutants retain the dimeric nature, albeit with a somewhat increased hydrodynamic radius that results in a small but significant decrease in their electrophoretic mobility compared to that of the wild-type enzyme (Figure 1A). We have checked that the contribution of the active site Lys and Asp residues to the global surface charge of the protein molecule is negligible under our experimental conditions. Thus, we cannot expect easily detectable changes in the electrophoretic running pattern upon mutation of the active site Lys and Asp side chains into Ala itself. Therefore, the observed decrease in the electrophoretic mobilities of all the mutants (relative to the wild-type enzyme) might be due to a small perturbation of the tertiary and/or quaternary structure of the protein molecule. Changes in the relative positions of the two domains (e.g., domain opening) could equally lead to a unidirectional increase in the molecular dimensions and a consequent reduction of the electrophoretic mobility. Our SAXS measurements (cf. below), indeed, supported this proposal. At the same time, the near-UV CD spectra of the mutants exhibit slight but significant differences from that of the wild-type enzyme, consistent with small local changes in the tertiary structure upon mutation (Figure 1B). On the other hand, the far-UV CD spectra of the mutants do not differ from that of the wild-type enzyme, indicating the identities of their secondary structures (not shown). In agreement, all the mutants exhibited cooperative heat transitions by DSC calorimetry, with transition temperatures similar to that of the wild-type enzyme (not illustrated).

Effects of Mutation of the Active Site Residues on the Kinetic Properties of *Tt*-IPMDH. Table 1 summarizes the kinetic constants of the investigated single side-chain mutants of *Tt*-IPMDH as compared to the values characteristic of the wild-type enzyme. The largest decreases in the k_{cat} value have been observed in the cases of K185A and D241A mutants, both of them exhibiting only 0.06% of the wild-type enzyme activity. Activities of the other mutants decrease in the following order:

DOI: 10.1021/acs.biochem.5b00839
Biochemistry XXXX, XXX, XXX–XXX

N102A (13%) > D245A (10.5%) > Y139A (2.9%) > D217A (1.1%). The K_m values of the substrates do not show similarly large changes; only the K_m^{IPM} values of K185A and D241A mutants with the lowest catalytic activities increase appreciably, indicating weakening of the catalytic interactions with IPM. However, the $K_m^{NAD^+}$ values do not exhibit appreciable changes for either mutant, because all of the mutations are located in the IPM binding site. The only exception is the Y139A mutant that unexpectedly exhibits a significant decrease in its $K_m^{NAD^+}$, which is similar to the observations by Miyazaki and Oshima that were interpreted as an effect of some undefined local conformational changes in the NAD^+ binding site of this mutant.[52] It may be notable that previously we have detected a significant increase in $K_m^{NAD^+}$ in the case of mutation of E270, the glutamate side chain of which directly interacts with NAD^+. For comparison, the kinetic data of E270A are also listed in Table 1.

Figure 2 illustrates the positions and the interactions of the presently mutated side chains in the IPM binding site. Among them, K185′, D241, and D217′ (the prime denotes the positioning of the side chain in the other subunit of the dimer) contact the reacting OH group of the substrate IPM and Y139 contacts the C3-carboxylate of IPM. As expected, the directly contacting side chains of K185′, D241, D217′, and Y139 exhibit the greatest responsibility for enzyme activity. The side chains of N102 and D245 have smaller contributions to the enzyme activity and no direct contacts with the substrate.

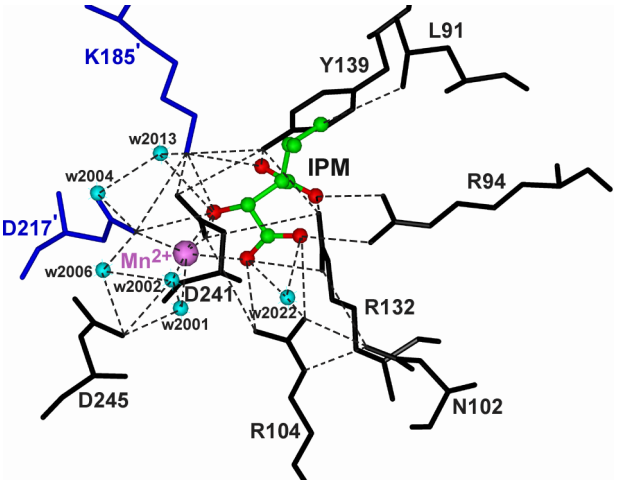

Figure 2. Structural details of binding of Mn^{2+}−IPM to *Tt*-IPMDH in the completely closed Mn^{2+}−IPM−NADH−IPMDH quaternary complex. Using the atomic coordinates of PDB entry 4F7I of the wild-type quaternary complex of *Tt*-IPMDH,[13] the substrate binding site is depicted as follows. The active site side chains are illustrated by black and blue stick models indicating their origins of different subunits. The substrate IPM is shown with ball and stick models, colored according to atom. Mn^{2+} and the water molecules bound in the active site are represented by purple and blue spheres, respectively. The dashed lines represent the atomic interactions (H-bonds and/or electrostatic interactions, defined in Materials and Methods; cf. Molecular Graphical Analysis of the X-ray Structure).

pH Dependence of the Enzyme Activities of the Active Site Mutants of *Tt*-IPMDH. Similar to other oxidative decarboxylases,[1] IPMDH functions via an acid−base catalysis; the pH dependence of the enzyme activity is an informative characteristic of this aspect. Previously, we have characterized this property of wild-type *Tt*-IPMDH and attributed it to the dissociation of an ionizable group with a p*K* of 7.4.[53] Here, the same analysis has been conducted with the investigated mutants (Figure 3), and the derived p*K* values are summarized in Table 1. Only the pH dependence of the activity of Y139A did not follow a simple ionization curve. Because the CD spectra of the enzymes [recorded in the pH range of 6−9 (not shown)] do not indicate any significant structural changes, the observed pH dependences of the activities can most probably be due to the ionization of at least one specific active site residue.

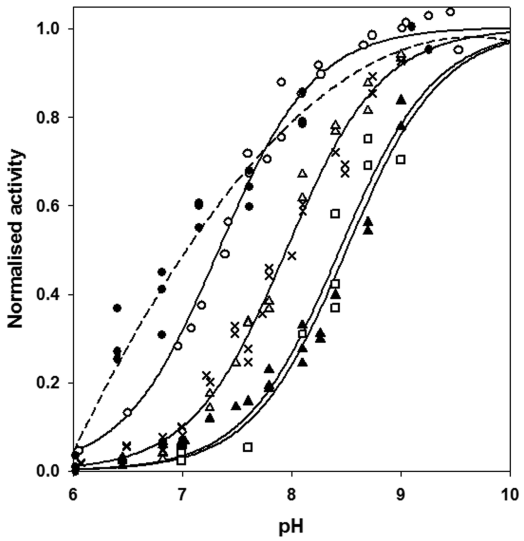

Figure 3. pH dependence of enzyme activities of various active site mutants of *Tt*-IPMDH in comparison to that of the wild-type enzyme. Enzyme activities of wild-type IPMDH (○) as well as mutants D241A (▲), D217A (×), D245A (△), K185A (□), and Y139A (●) are plotted as a function of pH after normalization of the data to the same maximal activities at high pH values. The data were fitted to eq 1 (—), and the obtained p*K* values are summarized in Table 1. The dashed line illustrates the pH dependence of activity of Y139A that does not follow a simple p*K* curve.

Remarkably, the two mutants (K185A and D241A) exhibiting the lowest catalytic activities are characterized by the largest shift of their p*K* values toward the more basic region. Moreover, the pH dependences of their activities are almost coincident. The first finding clearly supports our previous conclusion from a combined crystallographic and QM/MM modeling study that the ε-amino group of K185′ acts as a general base in the catalysis aiding the deprotonation reaction, prior to the transfer of the hydride from the substrate IPM to the nicotinamide ring of NAD^+[13] (Scheme 1). The closely similar pH dependences of the activities of K185A and D241A may indicate that the carboxylate of D241 acts cooperatively with K185′ in the abstraction of a proton from IPM, as also supported by the present QM/MM modeling study (cf. below). This proton relay system may be additionally aided by several H-bonding water molecules (cf. Figure 2, including the catalytic water, w2013[13]), located in the active site. Although the activity−pH profiles of the other two Asp mutants (D217A and D245A) are somewhat different, they both exhibit an intermediate p*K* value of 7.9. Still, the contributions of these two active site Asp residues and the interacting water molecules (Figure 2) to the proton relay system cannot be excluded.

No similar conclusion can be drawn from the unusual pH dependence of the activity of the Y139A mutant. The equivalent Y160 of *E. coli* ICDH was assumed to be a general

DOI: 10.1021/acs.biochem.5b00839
Biochemistry XXXX, XXX, XXX−XXX

Scheme 1. Complete Reaction Mechanism of the Catalytic Cycle by IPMDH[a]

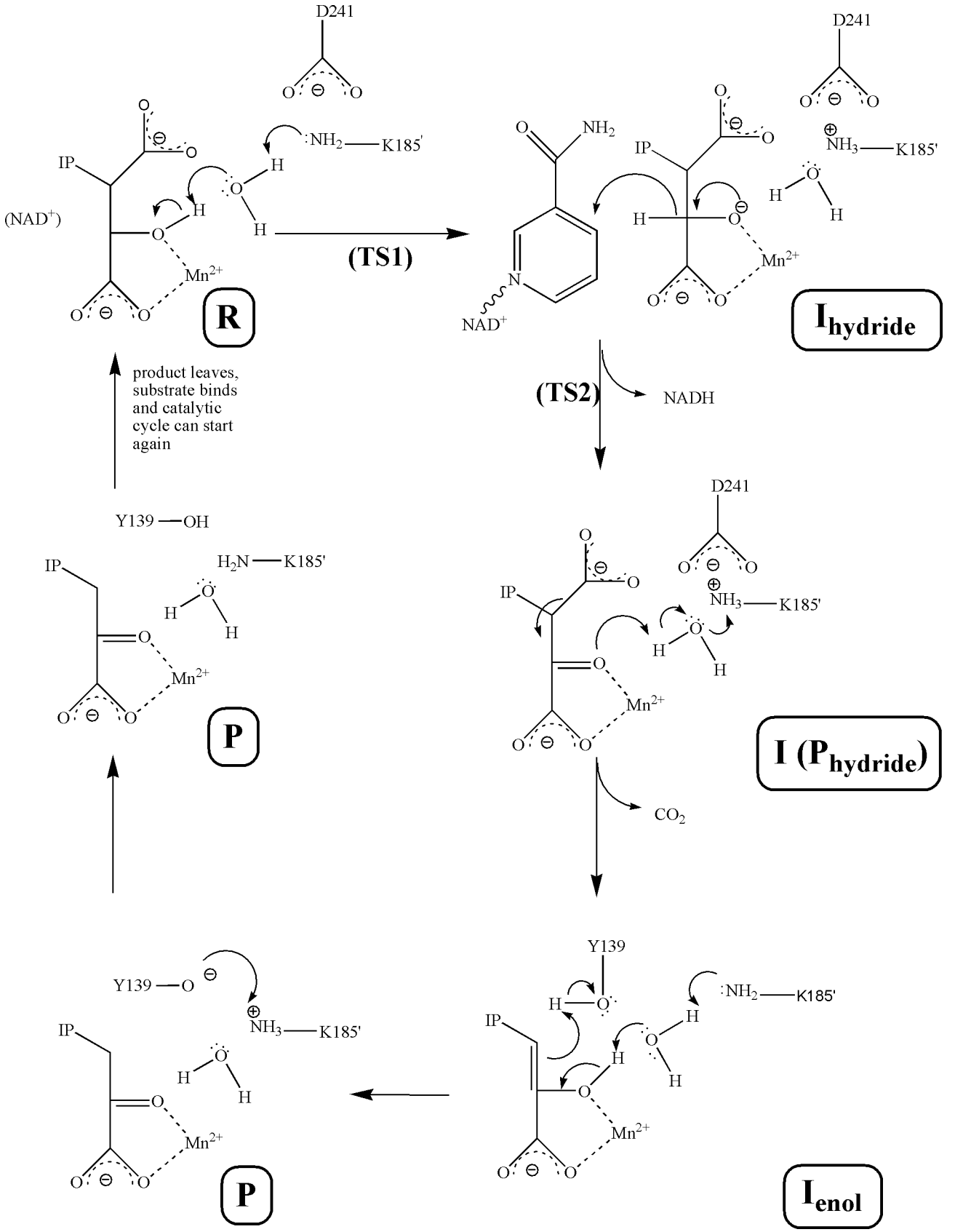

[a]IP represents the isopropyl group of IPM. R, I, and P represent the reactant, intermediate, and product states, respectively. It is notable that the product of the hydride transfer ($P_{hydride}$) is identical to the intermediate (I) state of the overall reaction. TS1 and TS2 indicate the transition states of the proton and hydride transfers, respectively.

DOI: 10.1021/acs.biochem.5b00839
Biochemistry XXXX, XXX, XXX−XXX

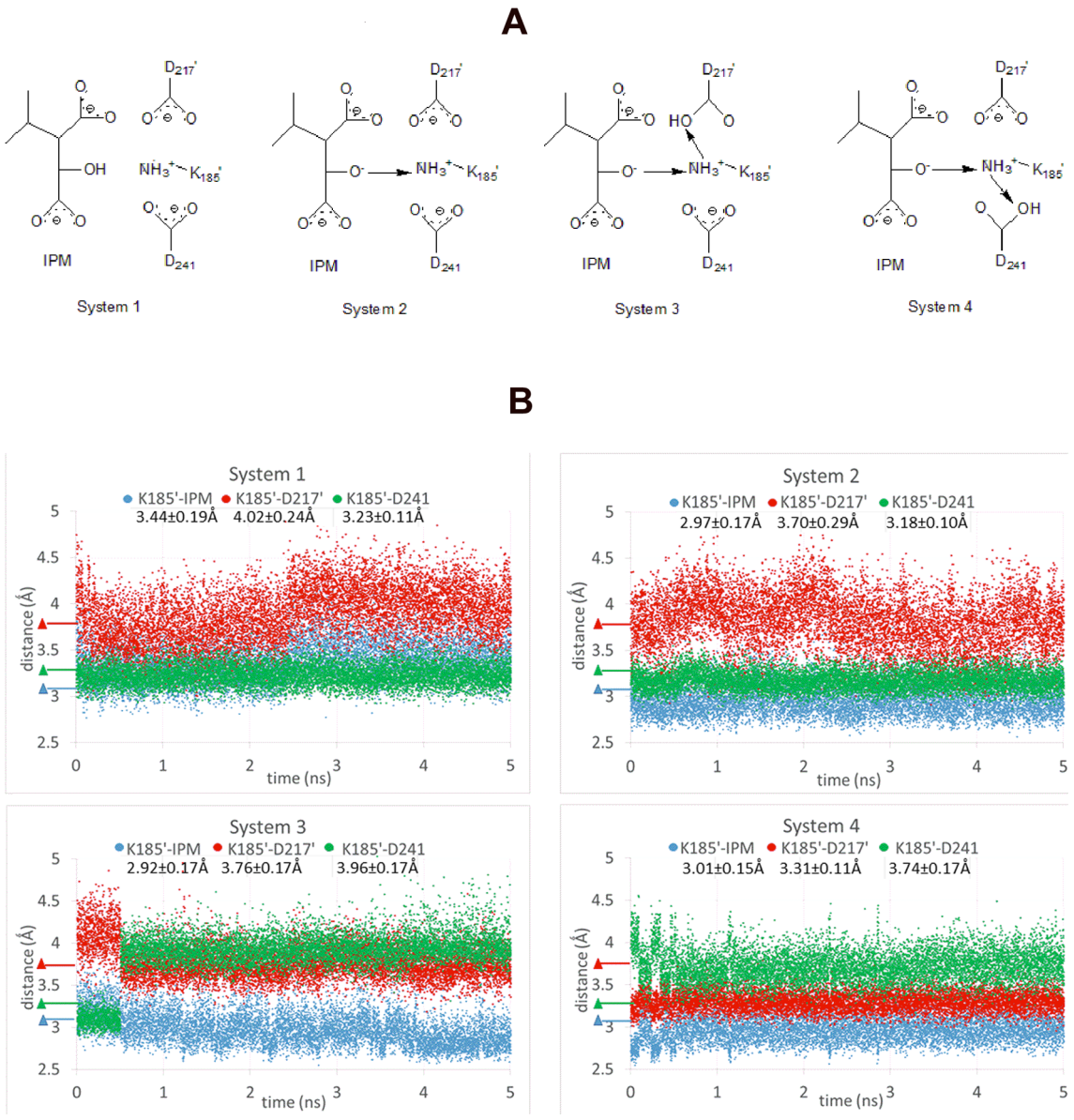

Figure 4. (A) Protonation states of IPM, K185, D217, and D241 in various systems studied by MD simulations and (B) changes in interatomic distances along the trajectory of the MD simulations in differently protonated systems. In panel A, the arrows indicate the directions of proton transfers that have occurred in the investigated systems. In panel B, in each case, the distances were measured from the ε-amino N atom of K185′ to the hydroxyl O atom of IPM (blue) or to the γ-carbon atom of D217′ (red) or D241 (green). In each diagram, the average distances measured during the last 2 ns of the simulations are numerically given together with their standard deviations. Along the y-axis colored triangles indicate the distance found in the corresponding X-ray structure (PDB entry 4F7I). Reference values are distances between ε-amino N atom of K185′ and (1) the hydroxyl O atom of IPM (3.05−3.07 Å), (2) the carboxylic carbon atom of D217′ (3.60−3.73 Å), and (3) the carboxylic carbon atom of D241 (3.23−3.38 Å).

acid in protonation of the enolate intermediate after the decarboxylation step (cf. Scheme 1); this may also hold for IPMDH.[1]

Determination of the Protonation State of K185 in the Resting State of the Enzyme. On the basis of the enzyme kinetic data, K185 is one of the most important residues involved in the catalytic cycle of IPMDH. In our previous work,[13] we suggested that it was unprotonated in the resting state of the enzyme. As K185 is a basic residue that is considered to be protonated at ambient pH values, we have sought to obtain further evidence to support our unusual hypothesis.

One important consideration lies in comparing the number of acidic (D217′, D241, and D245) and basic (R94, R104, and R132 apart from K185′) residues in the active site. Furthermore, there is a divalent cation (Mn^{2+}/Mg^{2+}) in the active site, which brings the overall charge of the active site to +2 even if K185′ is neutral. This significant positive charge in the active site is needed for efficient binding of the substrate IPM but does not seem to favor the presence of an extra positive charge on K185′. However, the situation dramatically changes when the IPM ligand (a dicarboxylic acid) binds the active site: its two carboxylate groups balance the original positive charge and generate better conditions for the protonation of K185′. This qualitative picture is well-supported

DOI: 10.1021/acs.biochem.5b00839
Biochemistry XXXX, XXX, XXX−XXX

by pK_a calculations by the PropKa program. The pK_a value of K185′ is predicted to be 5.9 in the absence and 8.1 in the presence of IPM in the active site, which suggests that K185′ becomes protonated upon ligand binding.

Our hypothesis regarding the protonation state of K185′ and the mechanism for abstraction of a proton from the substrate is in contrast to studies of other enzymes. In the case of malate dehydrogenase,[8] 6-phosphogluconate dehydrogenase, and various isocitrate-dehydrogenase enzymes, it has been proposed that the nearby lysine residue has to be first deprotonated by an aspartic acid residue to be able to act as a general base to remove the 2-hydroxyl proton of the substrate.

To decide which scenario is more likely to be valid in IPMDH, we have conducted molecular dynamics simulations on systems in various protonation states as shown in Figure 4A. Previously,[13] we have argued, on the basis of QM/MM calculations, that the proton transfer process from the hydroxyl group of IPM to K185′ is very facile and is likely to occur immediately upon IPM binding even if the other ligand, NAD^+, is not present. If this is the case, this would imply that in the crystal structure of the *Tt*-IPMDH−Mn^{2+}−IPM−NADH quaternary complex a deprotonated hydroxyl group of IPM and a protonated K185′ side chain should be present. As this structure should be distinguishable from other differently protonated systems, we conducted MD simulations to investigate which protonation state is the most consistent with the X-ray structure. System 1 corresponds to the reactant state structure proposed for analogous enzymes: the amino group of K185′ is protonated, and the hydroxyl group of IPM is neutral. System 2 matches our proposal: the originally neutral amino group of K185′ acted as a base and abstracted the proton from the hydroxyl group of IPM. Systems 3 and 4 are consistent with the proposal that K185′ is protonated in the resting state of the enzyme and in the course of the catalyzed reaction abstracted the proton from the hydroxyl group of IPM and transferred one of its protons to a nearby aspartic acid residue, either to D217 (system 3) or to D241 (system 4).

We have monitored the distances that are characteristic of the interactions among the amino group of K185′, the hydroxyl group of IPM, and the carboxylic groups of D217′ and D241. The results have been summarized in Figure 4B. It is obvious from the figure that the characteristic distances show very great variation with the protonation state of the studied residues, and only system 2 features distances consistent with the X-ray structure. In the case of system 2, all distances vary around the corresponding distances in the X-ray structure. In contrast, some major rearrangements are observed for the other systems. For example, in the case of system 1, the distance between the amino nitrogen atom of K185′ and the hydroxyl oxygen of IPM increases to ∼3.5 Å in contrast to the experimental value of 3.07 Å. Furthermore, the hydroxyl group of IPM turns away from K185′, and the hydroxyl hydrogen is found in a very unfavorable position for the proton transfer to occur. The results of the MD simulations on systems 3 and 4 are even more inconsistent with the X-ray structure, where D241 is located closer to K185′ (the distances of the carboxylate O atoms from the Lys NZ atom are 3.30 and 2.62 Å) than to D217′ (the corresponding distances are 3.78 and 3.60 Å, respectively), but this order is reversed in these two model systems. Therefore, the results of the MD simulations strongly support the hypothesis that (1) in the resting state of the enzyme K185′ is unprotonated, (2) this residue is the final base responsible for the deprotonation of the hydroxyl group of IPM, and (3) D217′ or D241 are not directly involved in the proton transfer process.

As other members of the β-hydroxyacid oxidative decarboxylase family are thought to operate by a similar mechanism, we were interested to know whether the finding that the catalytically active lysine residue (K185′) is unprotonated in the resting state of IPMDH may be relevant to the other members of the enzyme family. Therefore, using the PropKa program, we predicted the pK_a value of the catalytically active lysine residues in related enzymes in the presence and absence of their substrates. In each case, we observed that in the presence of the substrate the pK_a value of the lysine residue is predicted to increase by ∼2 units, similar to the case for the IPMDH enzyme (see the details in the Supporting Information). This suggests that the unprotonated nature of the catalytic lysine residue might be a general feature of the β-hydroxyacid oxidative decarboxylase family.

Testing the Catalytic Role of the Active Site Side Chains by QM/MM Modeling. As mentioned above, IPMDH catalyzes a two-step reaction: the NAD^+-dependent reversible oxidation of IPM followed by an irreversible decarboxylation step (cf. Scheme 1). We showed earlier that the oxidation step itself is a sequential event of a proton transfer step and a hydride transfer step.[13] Starting from the reactant state (R), a proton from the hydroxyl group of IPM is transferred via a catalytic water molecule to K185′ involving a low-energy transition state (TS1) to form an intermediate ($I_{hydride}$). From this state, a hydride ion is transferred from C2 of IPM to NAD^+ via a second transition state (TS2) to form the 3-isopropyl-α-keto-glutarate product ($P_{hydride}$) of the oxidation step, which is itself the major intermediate (I) of the overall catalytic reaction and can undergo irreversible decarboxylation in the active site of the enzyme.

In the study presented here, we extended our calculations to rationalize the experimentally observed activities of the mutated enzymes. Herein, we could not study the effect of K185′ on the reaction mechanism, as it acts as the proton acceptor according to the proposed reaction mechanism and participates in a bond forming process, which can be modeled by only quantum mechanical methods. For this reason, this residue has to be included in the quantum mechanically described region; thus, its effect cannot be studied in the same manner as those of the other side chains. Most likely, the K185A mutant enzyme operates in a manner slightly different from that of the wild-type enzyme; the proton acceptor role of K185 could be taken over by one of the aspartate residues or possibly by a hydroxide ion. Some support for the latter hypothesis is provided by the fact that the pH optimum of the K185A enzyme is higher than that of the wild-type enzyme. This is evidenced by their pK profiles: for the mutant enzyme, it is shifted toward pH values (thus to higher hydroxide ion concentrations) higher than that of the wild-type enzyme.

Thus, using point-charge deletion analysis, we studied the effect of N102A, Y139A, D217A, D241A, and D245A mutations on the proton and hydride transfer steps of the catalytic reaction. This approach allowed us to determine whether the experimentally observed decrease in the k_{cat} values of the mutants is likely to originate from a direct effect or an indirect effect. In the first case, the residue has a major role in stabilizing the transition state, and this should be reflected in the obtained activation energies. However, indirect effects (e.g., when mutation perturbs the tertiary structure of the enzyme) cannot be captured by point-charge deletion analysis: they

DOI: 10.1021/acs.biochem.5b00839
Biochemistry XXXX, XXX, XXX−XXX

would require extended molecular dynamics simulations to identify the exact role of the residue in the tertiary structure and how it reduces the catalytic activity. Nevertheless, in real systems, a mixture of these effects may be the reason for the decreased catalytic activity.

Before we discuss the obtained results, it might be useful to touch upon the accuracy of our calculated data and emphasize that the obtained numbers give only qualitative insight and should not be taken literally. On the basis of the Arrhenius equation, the activation energy differences between the wild-type and mutant enzymes can be predicted from the experimental k_{cat} values (see Table 1). The data show that the experimentally observed reduced reaction rates do not always translate into a seriously increased energy of activation; e.g., the 13.9% activity of the N102A mutant corresponds to an only 1.1 kcal/mol increase in the activation energy. Unfortunately, this effect, even with very precise computational methods [e.g., with the CCSD(T) method, which is the gold standard of computational chemistry], cannot be expected to be described reliably. In light of the estimated activation energy differences in the various mutants, one can realistically expect the calculations to reproduce that of the D241A mutation as the most severe one; the Y139A and D217A mutants should have similar but less reduced activities, and the D245A and N102A mutations should have an even smaller effect on the catalytic reaction.

In Figure 5A, we have plotted the estimated relative energies of the most important structures involved in the proton and hydride transfer step. With the exception of the D241A and D217A mutants, all three profile calculations show exactly the same trend and the data are characterized by a very small standard deviation. However, the results with D241A and D217A are found to be contradictory. Two profiles (profiles 2 and 3 referring to our previous work with the wild-type enzyme[13]) suggested a more significant role for the D241A mutation than for the D217A mutation, in accordance with the experiment, but profile 1 predicted the opposite effect (cf. also eq 2). Therefore, we have carefully checked the structures, and we found that in the case of the structural model corresponding to profile 1 the interaction between D241 and K185′ is significantly different from that of the other two profiles as well as from that of the X-ray structure. As mentioned in the previous chapter, in the X-ray structure (as well as in the structural models for profiles 2 and 3), D241 is located definitely closer to K185′ than D217′, and both of the carboxylic oxygen atoms of D241 interact with K185′. In contrast in profile 1, D241 turned away from K185′; only one of its carboxylate oxygen atoms remained in the vicinity, leading to false results. For this reason in Figure 5A for D217A and D241A, the data obtained from only profiles 2 and 3 are reported. In the case of both D217A and D241A, almost monotonously increasing relative energy curves are predicted by the calculations with an even greater effect for the D241A mutation, in accordance with the experiment. However, the monotonously increasing nature of the curves is apparently in contrast to the expectation that in a chemically viable reaction the energy of the transition state should be higher than that of the product (e.g., compare TS2 with Phydride). It is important to emphasize that the obtained numbers do not describe the exact thermodynamical properties of the mutant enzymes; instead, they shed light on the electrostatic effect of the investigated amino acids in the wild-type enzyme, from which one may obtain an approximate view on the functioning of the mutant enzymes. This means that when D241 or D217′ is replaced with Ala a very important stabilizing group is removed from the active site of the enzyme, which leads to very high relative energies of the states involved in the hydride transfer step ($I_{hydride}$, TS2, and $P_{hydride}$) and that this effect not only is essential in the transition state but also contributes to the stabilization of the Phydride state, which is the intermediate of the overall catalytic cycle. This implies that these groups are essential for the proper functioning of the enzyme in accordance with the results of activity measurements, which showed very low activities for these mutants [D217A, 1.1%; D241A, 0.06% (cf. Table 1)]. Within the accuracy of the calculations, the activity difference between these two mutants is reasonably well reproduced. The fact that the chemical reaction occurs in these mutant enzymes suggests that most likely the intermediate and transition state structures of the mutant enzymes are different from those of the wild type; i.e., new reaction routes might be opened to compensate for the effect of the mutations. However, these possibilities were outside of the scope of the modeling presented here.

In Figure 5B, we have pictorially demonstrated the basis for the considerable catalytic effect of these two side chains in the WT enzyme. In the reactant state, K185′ is neutral and interacts via hydrogen bonding interactions with D217′ and D241. These interactions increase the basicity of K185′, which can deprotonate the hydroxyl group of IPM via TS1 leading to $I_{hydride}$, which in turn is stabilized by numerous favorable electrostatic interactions. When D217′ or especially D241,

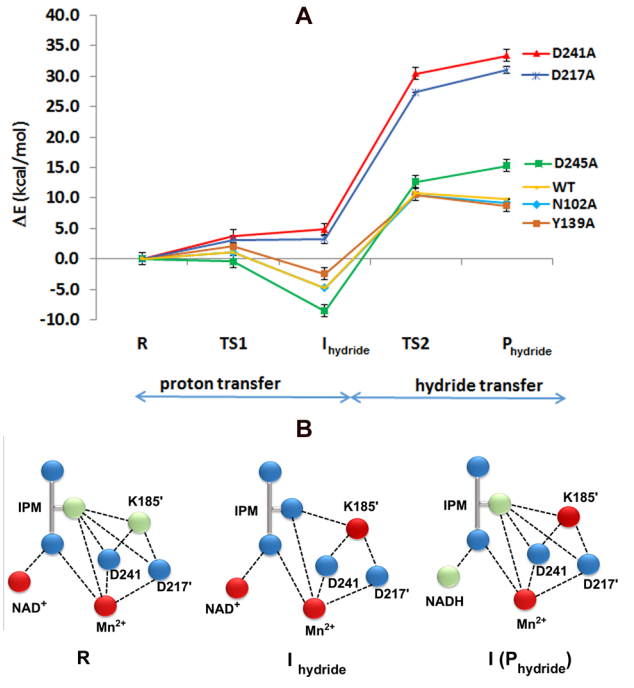

Figure 5. Results and interpretation of the QM/MM calculations. The estimated relative energies with their standard deviations ($\Delta E_{state}^{mutant}$; cf. eq 3) of the various states (reactant R, transition states TS1 and TS2, intermediate $I_{hydride}$, and product $P_{hydride}$) of the proton and hydride transfer reactions of the mutant variants of *Tt*-IPMDH are represented in panel A. The major electrostatic interactions of the active site are illustrated in panel B in the reactant (R) and the intermediate ($I_{hydride}$) states during the hydride transfer reaction. The differently charged groups are colored differently (green, neutral; blue, negative; and red, positive).

DOI: 10.1021/acs.biochem.5b00839
Biochemistry XXXX, XXX, XXX−XXX

Table 2. Comparison of SAXS Experimental Data of the *Tt*-IPMDH−Mn^{2+}−IPM−NADH Quaternary Complex with Those Derived from the Crystallographic Models

	R_g (Å)[a]		discrepancy[d] values χ between the scattering from crystallographic models and experimental data			volume fractions of open/closed structures[f]	
	GNOM method	Guinier method	closed crystal structure	open crystal structure	open/closed mixture[e]	V_{closed} (%)	V_{open} (%)
wild type	27.4 ± 0.2	27.4 ± 0.3	1.18	1.19	**1.09**	53 ± 3	47 ± 3
K185A mutant	28.1 ± 0.2	28.2 ± 0.3	2.26	1.19	**1.15**	15 ± 3	85 ± 3
Y139A mutant	27.6 ± 0.2	27.7 ± 0.3	1.53	1.28	**1.22**	46 ± 3	54 ± 3
D217A mutant	28.4 ± 0.2	28.5 ± 0.3	2.41	**1.22**	1.22	0	100
D241A mutant	28.4 ± 0.2	28.5 ± 0.3	2.49	**1.26**	1.26	0	100
D245A mutant	27.9 ± 0.2	28.0 ± 0.3	2.16	1.41	**1.32**	32 ± 3	68 ± 3
N102A mutant	28.2 ± 0.2	28.3 ± 0.3	2.32	1.36	**1.16**	22 ± 3	78 ± 3
E270A mutant[b]	28.4 ± 0.2	28.5 ± 0.3	1.71	1.08	1.07	5 ± 3	95 ± 5
R_g (theoretical) (Å)[c]	26.67	28.45					
molecular mass (kDa)[c,g]	74.3	73.8					

[a]The R_g values were computed by two alternative methods, using the program GNOM and Guinier approximation. [b]Published previously.[57] [c]Values of the high-resolution models as retrieved from PDB entry 4F7I for the closed crystal structure of the *Tt*-IPMDH−Mn^{2+}−IPM−NADH quaternary complex and PDB entry 2Y3Z for the open crystal structure of apo *Tt*-IPMDH. [d]The minimum values of discrepancy (in bold) indicate the best correlation between SAXS data and crystallographic model. [e]The fits for open/closed mixture were obtained with OLIGOMER. [f]V_{open} and V_{closed} correspond to the volume fractions of each state found by OLIGOMER. [g]The small variations in the calculated molecular mass are due to different numbers of residues resolved in different crystal structures.

which is closer to K185′, is replaced with Ala, the basicity of K185′ is expected to drop dramatically because of the loss of significant electrostatic interactions stabilizing the $I_{hydride}$ state, and the decreased basicity will lead to a significant increase in the activation energy of the proton transfer reaction (as shown by the calculations) and decrease the reactivity of the enzyme (as witnessed by the experimental data).

In the case of the D245A mutant, the intermediate state seems to be more stable than in the WT enzyme, while the TS2 and $P_{hydride}$ states are slightly destabilized. As a consequence, the activation energy of the rate-determining hydride transfer step is considerably larger than in the case of the WT, in accordance with the experimentally observed reduced activity [10.9% (cf. Table 1)] of the D245A mutant. One of the possible roles of the D245 residue might be hindering an overly strong stabilization of the $I_{hydride}$ state, thereby decreasing the energy of activation of the hydride transfer step.

The calculated relative energies of the N102A mutant are almost identical to those obtained for the WT enzyme. This implies that residue N102 does not contribute significantly to the electrostatic catalysis in IPMDH, which is in accordance with the fact that this mutant retained the highest activity [13.9% (cf. Table 1)] among those of the studied mutants, and the decrease in activity is due most likely to the role of the N102 side chain in stabilizing the closed conformation, as demonstrated below by the SAXS measurements (cf. Table 2).

The QM/MM calculations do not explain the seriously impaired activity [2.7% (cf. Table 1)] of the Y139A mutant. According to the calculations, the proton and hydride transfer steps in the enzyme should be as facile in this mutant as in the WT, in contrast to the experimentally observed 50-fold decrease in reactivity. However, the calculations capture only the electrostatic effect of the amino acid residues in the proton and hydride transfer step of the reaction (cf. Materials and Methods); they do not account for hindrance of the decarboxylation step or for changes in the tertiary structure. In the case of the Y139A mutant, both factors might be relevant, as tyrosine requires a space considerably larger than alanine does, which could lead to some changes in the active site architecture. However, a more plausible scenario is that Y139 acts as the proton source in the enol−keto tautomerization process in the decarboxylation step of the reaction as suggested for similar enzymes.[1] When it is not present, the decarboxylation step becomes rate-limiting, leading to decreased activity, but this effect cannot be reproduced by the calculations. This hypothesis is supported by the fact that the p*K* profile of the Y139A mutant is distinctly different from those of the wild type and other mutants, whose p*K* profiles follow a simple ionization curve but are shifted compared to each other, suggesting that these systems have the same pH-dependent rate-limiting step. The fact that the p*K* profile of Y139A is different may indicate that in this mutant the step that follows the hydride transfer (possibly the decarboxylation) becomes the rate-limiting one.

On the basis of the computational and experimental results, we suggest the catalytic cycle shown in Scheme 1. In the first step of the reaction, a proton is abstracted by K185′ from the hydroxyl group of IPM, which is followed by the hydride transfer step. These two processes are strongly assisted by the D241 and D217′ residues, with D241 being even more influential. In the decarboxylation step, Y139 protonates C3 of the enol to form the final product, i.e., the keto form. The resting state of the enzyme might be regained by the reprotonation of Y139 by K185′, although other protonation pathways may exist for restoring the resting state of the enzyme.

Effects of the Active Site Mutation on the FRET Spectrum of *Tt*-IPMDH. Characteristic changes in the fluorescence emission spectrum of the complex of *Tt*-IPMDH and NADH were observed because of the occurrence of FRET from the Trp side chain(s) of IPMDH to the bound NADH.[10] This phenomenon, however, occurs only when the enzyme is complexed with its substrate, the metal ion complex of IPM that stabilizes the closed (active) conformational state of the enzyme;[14] therefore, FRET is thought to be a characteristic for the domain-closed conformation. This was supported by our previous SAXS measurements,[37] although an exceptional case was also discovered.[57]

Because the native gel electrophoresis experiment and the near-UV CD spectral changes observed upon the present

DOI: 10.1021/acs.biochem.5b00839
Biochemistry XXXX, XXX, XXX−XXX

mutations (cf. above) raised the possibilities of conformational changes upon mutations, we tested formation of the FRET with all the active site mutants of IPMDH mentioned above. Figure 6 illustrates the FRET spectra of each active site mutant and of the previously investigated mutant E270A, compared to those of the wild-type enzyme. Each mutation led to a reduction in the FRET spectrum, but to various extents, fluorescence intensities decreased in the following order: wild type > Y139A > D245A ≅ N102A > K185A > E270A > D217A = D241A. The complete absence of FRET spectra could be observed only in cases of the last two Asp mutants (D241 and D217′). These two aspartates are interacting directly with both the catalytic Mn^{2+} and the catalytic side-chain K185′ (cf. Figure 2).

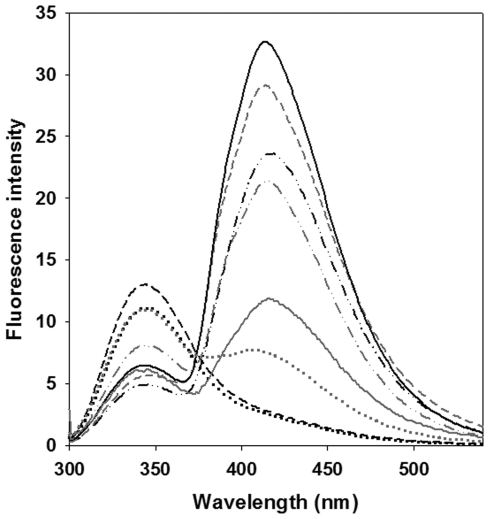

Figure 6. FRET spectra of the investigated active site mutants of *Tt*-IPMDH in comparison to that of the wild-type enzyme. FRET experiments with the wild type and various single mutants of IPMDH were conducted as described in Materials and Methods. The FRET spectra are illustrated by using the same types of lines as in the case of CD spectra in Figure 1B. As a comparison, FRET spectra of the previously investigated E270A mutant[57] (gray dotted line) and N102A (gray dash−dot−dot line) are also illustrated.

Domain Closure of *Tt*-IPMDH Is Prevented upon Mutation of the Active Site Residues: SAXS Measurements. To test whether domain closure is restricted or prevented in the cases of the mutants exhibiting the partial or complete absence of FRET spectra (cf. above), SAXS measurements have been taken. SAXS is the most appropriate method for testing protein conformational changes occurring in solution if they are accompanied by changes in the shape of the molecule, such as domain closure. The occurrence of domain closure was detected by SAXS in our previous studies with wild-type *Tt*-IPMDH in the complex with Mn^{2+}-IPM;[37] this experiment was repeated for all the mutants mentioned above. Table 2 summarizes the calculated R_g values as well as the extent of domain closure as expressed by the percentage of the open and closed forms estimated in the manner described in Materials and Methods. The results clearly show that, in addition to the previously demonstrated role of E270, the side chains of K185′, D217′, D241, and N102 make contributions to the formation of the active domain-closed conformation. The structural basis of these effects is illustrated below (cf. next section). The results especially emphasize the importance of N102 in domain closure, in spite of the relatively small

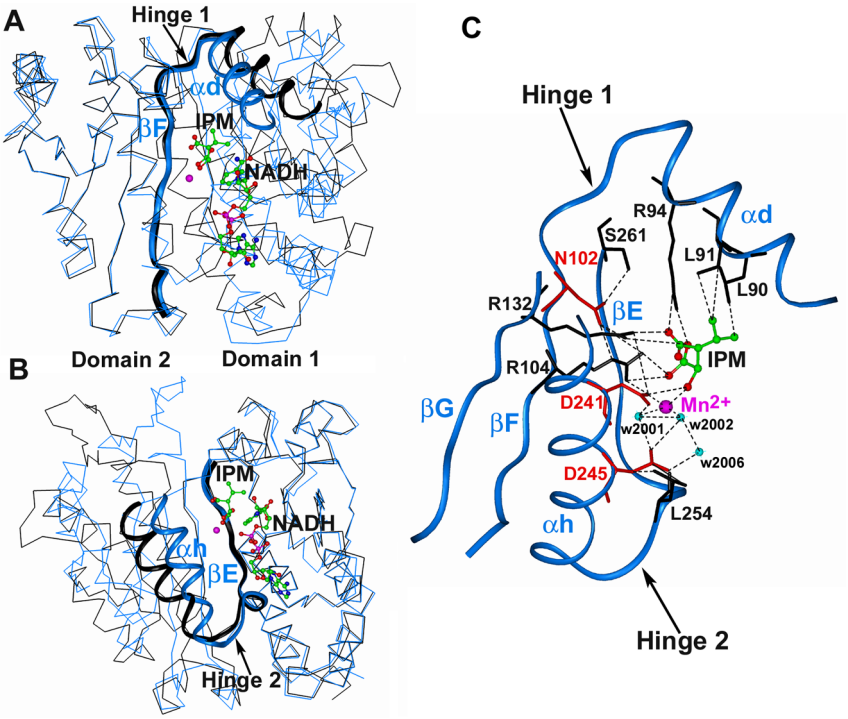

Figure 7. Illustration of the important hinges in the structure of *Tt*-IPMDH. The positions of (A) hinge 1 and (B) hinge 2 are shown in the whole subunit (Cα traces) by superimposing β-sheets F and E, respectively, of the open (black) and closed (blue) structures. The bound substrates are illustrated as ball and stick models, colored according to atom type. (C) Details of atomic interactions around both hinges are illustrated by dashed lines. The mutated side chains are labeled in red. This figure was prepared by using the atomic coordinates of PDB entry 4F7I of the wild-type quaternary complex of *Tt*-IPMDH.[13]

DOI: 10.1021/acs.biochem.5b00839
Biochemistry XXXX, XXX, XXX−XXX

calculated increase in the activation energy of proton transfer (Figure 5A) upon its mutation to alanine. In fact, the N102A mutant exhibits definitely reduced enzyme activity (cf. Table 1).

The good correlation between the data from SAXS and FRET measurements indicates that for the mutants exhibiting no or largely reduced FRET spectra domain closure ability is also impaired. Our FRET and SAXS experiments with the various active site mutants have revealed that the easily detectable effects of the bound substrates (mainly Mn^{2+}-IPM) in stabilizing the active domain-closed conformation of the wild-type enzyme are largely prevented upon selective mutation of the presently investigated catalytically important active site side chains.

Molecular Graphical Analysis Enlightens the Role of the Mutated Active Site Residues in Domain Closure. Previously, two main hinge regions were identified from comparison of the substrate-free and IPM-bound structures of *Tt*-IPMDH.[14] The locations of these hinges, namely, hinge 1 between αd and βF and hinge 2 between αh and βE, are illustrated in panels A and B of Figure 7, where the structures of the completely closed unproductive *Tt*-IPMDH−Mn^{2+}−IPM−NADH quaternary complex[13] and of the completely open apoenzyme[14] are superimposed. As noted earlier, binding of IPM itself facilitates the relative movement of αd toward βF via interacting side chains (L90, L91, and R94 from αd and R104 from βF), which is basically the operation of hinge 1 (Figure 7C). In addition, by interacting with D241 and D245 (αh), IPM mediates the movement of αh relative to central parallel β-strands E−G in the interdomain region, including operation of hinge 2 (cf. Figure 7C). This latter conformational change is also aided by transmission of the conformational signal through the side chains R132(βG) → N102(βF) → S261(βE). Moreover, D241(αh) interacts with R132(βG) as well as D245(αh) interacts with L254(βE). Most of these interactions are partially present in the *Tt*-IPMDH−Mn^{2+}−IPM ternary complex[14] but are complete only in the *Tt*-IPMDH−Mn^{2+}−IPM−NADH quaternary complex[13] when these interactions stabilize the closed states of both hinges 1 and 2.

The third investigated Asp of the active site, D217′, resides on helix αg′ of the other subunit (Figure 8). Interaction of IPM with this residue along with D241(αh) can contribute to stabilization of subunit interactions. As pointed out previously, the subunit−subunit interactions, operating within the dimer, result in further stabilization of the domain-closed conformation, and domain closure is completed only in the dimeric form.[14] The other catalytic side chain, K185′, is also located in the other subunit in a loop between αf′ and βI′, and by being inserted into the active site, it may stabilize the subunit−subunit interactions and thereby the domain-closed form, too. That probably occurs through its simultaneous electrostatic interactions with both D241 and D217′ and through its interactions with Y139 (cf. Figure 8B).

The other investigated residue, Y139, has been observed to undergo a simultaneous shift and rotation of its ring during domain closure.[14] It occupies a position on a loop preceding βK and βL, i.e., the constituents of the interacting arms of the subunits. In the domain-closed form, the side chain of Y139 is interacting simultaneously with active site residues R132(βG) and D241(αh) (cf. Figure 2). Thereby, it can contribute (although less effectively than the active site Asp residues) to stabilization of the domain-closed form and to interdomain communication.

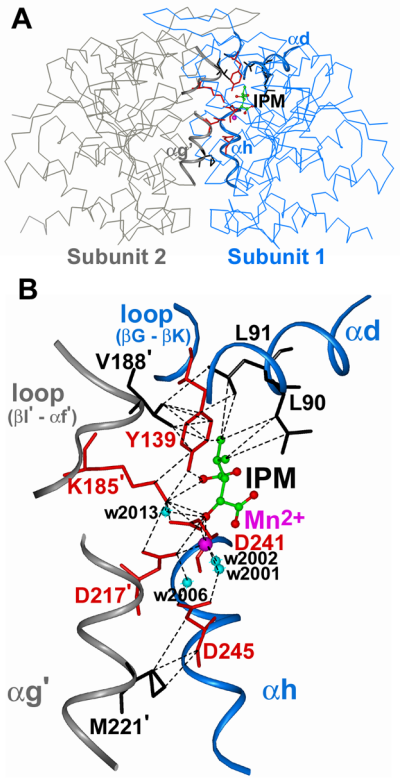

Figure 8. Illustration of the dimeric structure (A) and some of the atomic details of subunit interactions of *Tt*-IPMDH (B). The interaction of the two subunits (Cα traces) of IPMDH is shown in panel A. The contacting secondary structural elements are illustrated as ribbons. The details of the latter ones, including the bound substrate, are enlarged in panel B. The mutated side chains are labeled in red. This figure was prepared by using the atomic coordinates of PDB entry 4F7I of the wild-type quaternary complex of *Tt*-IPMDH.[13]

The side chain of N102 discussed above, which is not a direct substrate binding residue, seems to be more important in the transmission of the conformational signal between the domains, as suggested previously[14] and illustrated in Figure 7C. Indeed, the side chain of N102 contributes to stabilization of the closed conformation as demonstrated by the SAXS data (Table 2).

In summary, the structural analysis provides insight into the possible roles of the investigated active site side chains in domain closure. These mechanistic suggestions are supported by the results of the physicochemical investigations presented above, such as FRET and SAXS.

CONCLUSIONS

The enzyme kinetics and the various physicochemical experiments with the investigated point mutants of the active site of *Tt*-IPMDH led to the identification of the catalytic residues. Our thorough experimental studies (including enzyme kinetics and physicochemical investigations), complemented by molecular dynamics simulations and QM/MM calculations, have suggested that the side chains of K185′, D241, D217′, and Y139 significantly contribute to IPMDH catalysis. Thus, the mechanism seemingly fulfills the criteria formulated previously for other β-hydroxy acid oxidative decarboxylases. Furthermore, by analogy of their mechanisms, these results with IPMDH cleared up the previous uncertainties concerning identification of the catalytic residues in the case of isocitrate dehydrogenase.

DOI: 10.1021/acs.biochem.5b00839
Biochemistry XXXX, XXX, XXX−XXX

In addition, IPMDH as a dimer represents a unique example of the functionally related domain motions, in which the main catalytic residues are simultaneously responsible for both strengthening the subunit interactions and operation of the main hinges. Until now, there have been only a few studies in the literature about oligomeric proteins that indicate the possible relationship among domain motions, subunit−subunit interactions, and the proper steric arrangement of the active site residues.[58−61]

■ ASSOCIATED CONTENT

Supporting Information

The Supporting Information is available free of charge on the ACS Publications website at DOI: 10.1021/acs.biochem.5b00839.

Details about the methodology of the applied MD simulation as well as about the estimated pK_a values of the active site Lys residues in the enzyme−substrate complexes of various oxidative decarboxylases (PDF)

■ AUTHOR INFORMATION

Corresponding Authors

*Department of Inorganic and Analytical Chemistry, Budapest University of Technology and Economics, Gellért tér 4., H-1111 Budapest, Hungary. Phone: +36 1 4631 286. E-mail: julianna.olah@mail.bme.hu.

*Institute of Enzymology, Research Centre for Natural Sciences, Hungarian Academy of Sciences, Magyar tudósok krt. 2., H-1117 Budapest, Hungary. Phone: +36 1 3826 773. E-mail: vas.maria@ttk.mta.hu.

Present Address

#P.V.K.: Laboratory of reflectometry and small-angle scattering, Institute of Crystallography RAS, Leninsky pr. 59, 119333 Moscow, Russia.

Author Contributions

É.G. and T.S. contributed equally to this work.

Funding

Grant OTKA (NK 108642) of the Hungarian National Research Fund supported this work. Synchrotron facilities of EMBL (Hamburg Outstation) at the beamline at the DORIS storage ring, DESY, were used and supported by the funding from the European Community's Seventh Framework Programme (FP7/2007-2013) under Grant Agreement No. 226716 and from the German Ministry of Education and Science (BMBF) project BIOSCAT, Grant 05K20912. J.O. was supported by the Bolyai János Research Scholarship, and A.L. was supported by the Richter Gedeon Talentum Foundation fellowship.

Notes

The authors declare no competing financial interest.

■ ABBREVIATIONS

IPMDH, 3-isopropylmalate dehydrogenase (EC 1.1.1.85); *Tt*, *T. thermophilus*; IPM, (2*R*,3*S*)-3-isopropylmalate; FRET, Förster resonance energy transfer; HEPES, 4-(2-hydroxyethyl)-piperazine-1-ethanesulfonic acid; MES, 2-(*N*-morpholino)-ethanesulfonic acid; MOPS, 3-(*N*-morpholino)propanesulfonic acid; SAXS, small-angle X-ray scattering; SDS−PAGE, sodium dodecyl sulfate−polyacrylamide gel electrophoresis.

■ REFERENCES

(1) Aktas, D. F., and Cook, P. F. (2009) A lysine-tyrosine pair carries out acid-base chemistry in the metal ion-dependent pyridine dinucleotide-linked beta-hydroxyacid oxidative decarboxylases. *Biochemistry 48*, 3565−3577.

(2) Tao, X., Yang, Z., and Tong, L. (2003) Crystal structures of substrate complexes of malic enzyme and insights into the catalytic mechanism. *Structure 11*, 1141−1150.

(3) Malik, R., and Viola, R. E. (2010) Structural characterization of tartrate dehydrogenase: a versatile enzyme catalyzing multiple reactions. *Acta Crystallogr., Sect. D: Biol. Crystallogr. 66*, 673−684.

(4) Goncalves, S., Miller, S. P., Carrondo, M. A., Dean, A. M., and Matias, P. M. (2012) Induced fit and the catalytic mechanism of isocitrate dehydrogenase. *Biochemistry 51*, 7098−7115.

(5) Grodsky, N. B., Soundar, S., and Colman, R. F. (2000) Evaluation by site-directed mutagenesis of aspartic acid residues in the metal site of pig heart NADP-dependent isocitrate dehydrogenase. *Biochemistry 39*, 2193−2200.

(6) Kim, T.-K., Lee, P., and Colman, R. F. (2003) Critical role of Lys212 and Tyr140 in porcine NADP-dependent isocitrate dehydrogenase. *J. Biol. Chem. 278*, 49323−49331.

(7) Huang, Y. C., Grodsky, N. B., Kim, T. K., and Colman, R. F. (2004) Ligands of the Mn2+ bound to porcine mitochondrial NADP-dependent isocitrate dehydrogenase, as assessed by mutagenesis. *Biochemistry 43*, 2821−2828.

(8) Karsten, W. E., Liu, D., Rao, G. S., Harris, B. G., and Cook, P. F. (2005) A catalytic triad is responsible for acid-base chemistry in the Ascaris suum NAD-malic enzyme. *Biochemistry 44*, 3626−3635.

(9) Lee, M. E., Dyer, D. H., Klein, O. D., Bolduc, J. M., Stoddard, B. L., and Koshland, D. E., Jr. (1995) Mutational analysis of the catalytic residues lysine 230 and tyrosine 160 in the NADP+-dependent isocitrate dehydrogenase from Escherichia coli. *Biochemistry 34*, 378−384.

(10) Dean, A. M., and Dvorak, L. (1995) The role of glutamate 87 in the kinetic mechanism of Thermus thermophilus isopropylmalate dehydrogenase. *Protein Sci. 4*, 2156−2167.

(11) Miyazaki, K., Kakinuma, K., Terasawa, H., and Oshima, T. (1993) Kinetic analysis on the substrate specificity of 3-isopropylmalate dehydrogenase. *FEBS Lett. 332*, 35−36.

(12) Fujita, M., Toyooka, Y., Tamegai, H., Eguchi, T., and Kakinuma, K. (2000) Arg-94 is crucial to the catalysis of 3-isopropylmalate dehyrdogenase from Thermus thermophilus HB8. *J. Mol. Catal. B: Enzym. 9*, 149−155.

(13) Palló, A., Oláh, J., Gráczer, E., Merli, A., Závodszky, P., Weiss, M. S., and Vas, M. (2014) Structural and Energetic Basis of Isopropylmalate Dehydrogenase Enzyme Catalysis. *FEBS J. 281*, 5063−5076.

(14) Gráczer, É., Merli, A., Singh, R. K., Karuppasamy, M., Závodszky, P., Weiss, M. S., and Vas, M. (2011) Atomic level description of the domain closure in a dimeric enzyme: Thermus thermophilus 3-isopropylmalate dehydrogenase. *Mol. BioSyst. 7*, 1646−1659.

(15) Gibbs, A. C. (2014) Elements and modulation of functional dynamics. *J. Med. Chem. 57*, 7819−7837.

(16) Darrouzet, E., Moser, C. C., Dutton, P. L., and Daldal, F. (2001) Large scale domain movement in cytochrome bc(1): a new device for electron transfer in proteins. *Trends Biochem. Sci. 26*, 445−451.

(17) Bienert, R., Zimmermann, B., Rombach-Riegraf, V., and Graber, P. (2011) Time-dependent FRET with single enzymes: domain motions and catalysis in H(+)-ATP synthases. *ChemPhysChem 12*, 510−517.

(18) Yang, W. (2010) Lessons learned from UvrD helicase: mechanism for directional movement. *Annu. Rev. Biophys. 39*, 367−385.

(19) Shen, T., Tai, K., Henchman, R. H., and McCammon, J. A. (2002) Molecular dynamics of acetylcholinesterase. *Acc. Chem. Res. 35*, 332−340.

DOI: 10.1021/acs.biochem.5b00839
Biochemistry XXXX, XXX, XXX−XXX

(20) Masaike, T., Mitome, N., Noji, H., Muneyuki, E., Yasuda, R., Kinosita, K., and Yoshida, M. (2000) Rotation of F(1)-ATPase and the hinge residues of the beta subunit. *J. Exp Biol. 203*, 1−8.
(21) Kannan, N., Neuwald, A. F., and Taylor, S. S. (2008) Analogous regulatory sites within the alphaC-beta4 loop regions of ZAP-70 tyrosine kinase and AGC kinases. *Biochim. Biophys. Acta, Proteins Proteomics 1784*, 27−32.
(22) Nakanishi-Matsui, M., Sekiya, M., Nakamoto, R. K., and Futai, M. (2010) The mechanism of rotating proton pumping ATPases. *Biochim. Biophys. Acta, Bioenerg. 1797*, 1343−1352.
(23) Vas, M., Varga, A., and Gráczer, É. (2010) Insight into the mechanism of domain movements and their role in enzyme function: example of 3-phosphoglycerate kinase. *Curr. Protein Pept. Sci. 11*, 118−147.
(24) Palmai, Z., Seifert, C., Grater, F., and Balog, E. (2014) An allosteric signaling pathway of human 3-phosphoglycerate kinase from force distribution analysis. *PLoS Comput. Biol. 10*, e1003444.
(25) Owen, G. R., Stoychev, S., Achilonu, I., and Dirr, H. W. (2014) Phosphorylation- and nucleotide-binding-induced changes to the stability and hydrogen exchange patterns of JNK1beta1 provide insight into its mechanisms of activation. *J. Mol. Biol. 426*, 3569−3589.
(26) Yang, Z., Floyd, D. L., Loeber, G., and Tong, L. (2000) Structure of a closed form of human malic enzyme and implications for catalytic mechanism. *Nat. Struct. Biol. 7*, 251−257.
(27) Gerstein, M., and Echols, N. (2004) Exploring the range of protein flexibility, from a structural proteomics perspective. *Curr. Opin. Chem. Biol. 8*, 14−19.
(28) Bahar, I., Chennubhotla, C., and Tobi, D. (2007) Intrinsic dynamics of enzymes in the unbound state and relation to allosteric regulation. *Curr. Opin. Struct. Biol. 17*, 633−640.
(29) Henzler-Wildman, K. A., Lei, M., Thai, V., Kerns, S. J., Karplus, M., and Kern, D. (2007) A hierarchy of timescales in protein dynamics is linked to enzyme catalysis. *Nature 450*, 913−916.
(30) Gráczer, É., Varga, A., Melnik, B., Semisotnov, G., Závodszky, P., and Vas, M. (2009) Symmetrical refolding of protein domains and subunits: example of the dimeric two-domain 3-isopropylmalate dehydrogenases. *Biochemistry 48*, 1123−1134.
(31) Laemmli, U. K. (1970) Cleavage of structural proteins during the assembly of the head of bacteriophage T4. *Nature 227*, 680−685.
(32) Ornstein, L. (1964) Disc Electrophoresis. I. Background and Theory. *Ann. N.Y. Acad. Sci. 121*, 321−349.
(33) Konarev, P. V., Volkov, V. V., Sokolova, A. V., Koch, M. H. J., and Svergun, D. I. (2003) *PRIMUS*: a Windows PC-based system for small-angle scattering data analysis. *J. Appl. Crystallogr. 36*, 1277−1282.
(34) Guinier, A. (1939) La diffraction des rayons X aux trés petits angles; application á l'étude de phénoménes ultramicroscopiques. *Ann. Phys. 12*, 166−237.
(35) Svergun, D. I. (1992) Determination of the regularisation parameter in indirect-transform methods using perceptual criteria. *J. Appl. Crystallogr. 25*, 495−503.
(36) Svergun, D. I., Barberato, C., and Koch, M. H. J. (1995) CRYSOL - a program to evaluate X-ray solution scattering of biological macromolecules from atomic coordinates. *J. Appl. Crystallogr. 28*, 768−773.
(37) Gráczer, É., Konarev, P. V., Szimler, T., Bacsó, A., Bodonyi, A., Svergun, D. I., Závodszky, P., and Vas, M. (2011) Essential role of the metal-ion in the IPM-assisted domain closure of 3-isopropylmalate dehydrogenase. *FEBS Lett. 585*, 3297−3302.
(38) Brooks, B. R., Brooks, C. L., 3rd, Mackerell, A. D., Jr., Nilsson, L., Petrella, R. J., Roux, B., Won, Y., Archontis, G., Bartels, C., Boresch, S., Caflisch, A., Caves, L., Cui, Q., Dinner, A. R., Feig, M., Fischer, S., Gao, J., Hodoscek, M., Im, W., Kuczera, K., Lazaridis, T., Ma, J., Ovchinnikov, V., Paci, E., Pastor, R. W., Post, C. B., Pu, J. Z., Schaefer, M., Tidor, B., Venable, R. M., Woodcock, H. L., Wu, X., Yang, W., York, D. M., and Karplus, M. (2009) CHARMM: the biomolecular simulation program. *J. Comput. Chem. 30*, 1545−1614.
(39) Bash, P. A., Field, M. J., Davenport, R. C., Petsko, G. A., Ringe, D., and Karplus, M. (1991) Computer simulation and analysis of the reaction pathway of triosephosphate isomerase. *Biochemistry 30*, 5826−5832.
(40) Tian, B. X., and Eriksson, L. A. (2011) Catalytic mechanism and roles of Arg197 and Thr183 in the Staphylococcus aureus sortase A enzyme. *J. Phys. Chem. B 115*, 13003−13011.
(41) Liao, R. Z., and Thiel, W. (2013) Convergence in the QM-only and QM/MM modeling of enzymatic reactions: A case study for acetylene hydratase. *J. Comput. Chem. 34*, 2389−2397.
(42) Perez-Gallegos, A., Garcia-Viloca, M., Gonzalez-Lafont, A., and Lluch, J. M. (2014) A QM/MM study of the associative mechanism for the phosphorylation reaction catalyzed by protein kinase A and its D166A mutant. *J. Comput.-Aided Mol. Des. 28*, 1077−1091.
(43) Garcia-Viloca, M., Truhlar, D. G., and Gao, J. (2003) Reaction-path energetics and kinetics of the hydride transfer reaction catalyzed by dihydrofolate reductase. *Biochemistry 42*, 13558−13575.
(44) Szarek, P., Dyguda-Kazimierowicz, E., Tachibana, A., and Sokalski, W. A. (2008) Physical nature of intermolecular interactions within cAMP-dependent protein kinase active site: differential transition state stabilization in phosphoryl transfer reaction. *J. Phys. Chem. B 112*, 11819−11826.
(45) Cheng, Y., Zhang, Y., and McCammon, J. A. (2005) How does the cAMP-dependent protein kinase catalyze the phosphorylation reaction: an ab initio QM/MM study. *J. Am. Chem. Soc. 127*, 1553−1562.
(46) Warshel, A., Sharma, P. K., Kato, M., Xiang, Y., Liu, H., and Olsson, M. H. (2006) Electrostatic basis for enzyme catalysis. *Chem. Rev. 106*, 3210−3235.
(47) Harvey, J. N. (2004) Spin-forbidden CO ligand recombination in myoglobin. *Faraday Discuss. 127*, 165−177.
(48) Frisch, M. J., Trucks, G. W., Schlegel, H. B., Scuseria, G. E., Robb, M. A., Cheeseman, J. R., Scalmani, G., Barone, V., Mennucci, B., Petersson, G. A., Nakatsuji, H., Caricato, M., Li, X., Hratchian, H. P., Izmaylov, A. F., Bloino, J., Zheng, G., Sonnenberg, J. L., Hada, M., Ehara, M., Toyota, K., Fukuda, R., Hasegawa, J., Ishida, M., Nakajima, T., Honda, Y., Kitao, O., Nakai, H., Vreven, T., Montgomery, J. A., Jr., Peralta, J. E., Ogliaro, F., Bearpark, M., Heyd, J. J., Brothers, E., Kudin, K. N., Staroverov, V. N., Kobayashi, R., Normand, J., Raghavachari, K., Rendell, A., Burant, J. C., Iyengar, S. S., Tomasi, J., Cossi, M., Rega, N., Millam, N. J., Klene, M., Knox, J. E., Cross, J. B., Bakken, V., Adamo, C., Jaramillo, J., Gomperts, R., Stratmann, R. E., Yazyev, O., Austin, A. J., Cammi, R., Pomelli, C., Ochterski, J. W., Martin, R. L., Morokuma, K., Zakrzewski, V. G., Voth, G. A., Salvador, P., Dannenberg, J. J., Dapprich, S., Daniels, A. D., Farkas, Ö., Foresman, J. B., Ortiz, J. V., Cioslowski, J., and Fox, D. J. (2009) *Gaussian 09*, revision B.01, Gaussian, Inc., Wallingford, CT.
(49) Page, H. *Tinker: Software tools for molecular design* (http://dasher.wustl.edu/tinker/) (accessed 5 October, 2011).
(50) Olsson, M. H., Søndergaard, C. R., Rostkowski, M., and Jensen, J. H. (2011) PROPKA3: Consistent Treatment of Internal and Surface Residues in Empirical pKa predictions. *J. Chem. Theory Comput. 7*, 525−537.
(51) Søndergaard, C. R., Olsson, M. H., Rostkowski, M., and Jensen, J. H. (2011) Improved Treatment of Ligands and Coupling Effects in Empirical Calculation and Rationalization of pKa Values. *J. Chem. Theory Comput. 7*, 2284−2295.
(52) Miyazaki, K., and Oshima, T. (1993) Tyr-139 in Thermus thermophilus 3-isopropylmalate dehydrogenase is involved in catalytic function. *FEBS Lett. 332*, 37−38.
(53) Gráczer, É., Bacsó, A., Kónya, D., Kazi, A., Soós, T., Molnár, L., Szimler, T., Beinrohr, L., Szilágyi, A., Závodszky, P., and Vas, M. (2014) Drugs Against Mycobacterium Tuberculosis 3-Isopropylmalate Dehydrogenase Can be Developed using Homologous Enzymes as Surrogate Targets. *Protein Pept Lett. 21*, 1295−1307.
(54) Berdis, A. J., and Cook, P. F. (1993) Chemical mechanism of 6-phosphogluconate dehydrogenase from Candida utilis from pH studies. *Biochemistry 32*, 2041−2046.
(55) Price, N. E., and Cook, P. F. (1996) Kinetic and chemical mechanisms of the sheep liver 6-phosphogluconate dehydrogenase. *Arch. Biochem. Biophys. 336*, 215−223.

DOI: 10.1021/acs.biochem.5b00839
Biochemistry XXXX, XXX, XXX−XXX

(56) Quartararo, C. E., Hazra, S., Hadi, T., and Blanchard, J. S. (2013) Structural, Kinetic and Chemical Mechanism of Isocitrate Dehydrogenase-1 from Mycobacterium tuberculosis. *Biochemistry 52*, 1765−1775.
(57) Gráczer, É., Palló, A., Oláh, J., Szimler, T., Konarev, P. V., Svergun, D. I., Merli, A., Závodszky, P., Weiss, M. S., and Vas, M. (2015) Glutamate 270 plays an essential role in K(+)-activation and domain closure of Thermus thermophilus isopropylmalate dehydrogenase. *FEBS Lett. 589*, 240−245.
(58) Hayward, S., and Kitao, A. (2006) Molecular dynamics simulations of NAD+-induced domain closure in horse liver alcohol dehydrogenase. *Biophys. J. 91*, 1823−1831.
(59) Dey, S., Hu, Z., Xu, X. L., Sacchettini, J. C., and Grant, G. A. (2007) The effect of hinge mutations on effector binding and domain rotation in Escherichia coli D-3-phosphoglycerate dehydrogenase. *J. Biol. Chem. 282*, 18418−18426.
(60) Cunningham, C. N., Krukenberg, K. A., and Agard, D. A. (2008) Intra- and intermonomer interactions are required to synergistically facilitate ATP hydrolysis in Hsp90. *J. Biol. Chem. 283*, 21170−21178.
(61) Pemberton, T. A., Srivastava, D., Sanyal, N., Henzl, M. T., Becker, D. F., and Tanner, J. J. (2014) Structural studies of yeast Delta(1)-pyrroline-5-carboxylate dehydrogenase (ALDH4A1): active site flexibility and oligomeric state. *Biochemistry 53*, 1350−1359.
(62) Gráczer, É., Lionne, C., Závodszky, P., Chaloin, L., and Vas, M. (2013) Transient kinetic studies reveal isomerization steps along the kinetic pathway of Thermus thermophilus 3-isopropylmalate dehydrogenase. *FEBS J. 280*, 1764−1772.

DOI: 10.1021/acs.biochem.5b00839
Biochemistry XXXX, XXX, XXX−XXX